Direct determination of the contact area based on the concept of rounded indenter tip correction for Berkovich nanoindentation tests: Case study on silica glass

Xiaoying Guo[1], Danyu Jiang[2], Jianghong Gong[3,*]

[1]*School of Metallurgy and Materials Engineering, Liaoning Institute of Science and Technology, Benxi 117004, China*

[2]*State Key Laboratory of High Performance Ceramics and Superfine Microstructure, Shanghai Institute of Ceramics, Shanghai 200050, China*

[3]*State Key Laboratory of New Ceramics and Fine Processing, School of Materials Science and Engineering, Tsinghua University, Beijing 100084, China*

Received 23 December 2025; received in revised form 5 March 2026; accepted 27 March 2026

Abstract

Determination of the contact area is a key issue for extracting the mechanical properties from the analysis of nanoindentation load-displacement (P-h) curves. In this paper, a new method for the direct determination of the contact area with the empirical equation $A = C(h_c + h_d)^2$ was proposed. It is based on the consideration of round indenter tip correction, using the correction factor h_d yielded by fitting the loading segment of the measured P–h curve and the contact depth h_c determined from the unloading segment of the same curve. Thus, the mechanical properties can be extracted easily and directly without the need of the pre-calibration of area function. The applicability of this new method was examined by statistical analysis of a total of 497 nanoindentation tests performed on silica glass. It was shown that reliable results of Young's modulus and hardness can be obtained based on the proposed new method.

***Keywords**: mechanical properties, hardness, silica, nanoindentation*

I. Introduction

Nanoindentation technique has become a common approach for the mechanical characterisations of a variety of materials at submicron depths. The application of the analytical method established by Oliver and Pharr [1,2], usually called the OP method, makes this technique more attractive mainly due to the fact that the mechanical properties, such as Young's modulus and hardness, can be determined directly by analysing the recorded load-displacement (*P-h*) curve without the need to analyse image of the indenter impression.

The basic equation used in the OP method is:

$$S = \beta \frac{2}{\sqrt{\pi}} E_r \sqrt{A} \tag{1}$$

where S is the contact stiffness or the initial unloading slope (mN/nm), A is the projected contact area (nm^2) and $\beta = 1.058$ is a factor used to account for deviations in stiffness caused by the lack of axial symmetry for pyramidal indenters [2]. The reduced modulus E_r is defined by following equation:

$$\frac{1}{E_r} = \frac{1-\upsilon}{E} + \frac{1-\upsilon_I}{E_I} \tag{2}$$

where E (GPa) and υ are the Young's modulus and Poisson ratio of the test material, whereas E_I (GPa) and υ_I are the same parameters for the indenter.

The contact area A included in Eq. 1 is a function of the contact depth h_c (nm). For a perfect Berkovich indenter, the contact area can be calculated directly based on the indenter geometry [1]:

$$A = 24.5 h_c^2 \tag{3}$$

However, a real indenter is never perfectly sharp due to the restriction caused by the state-of-art of polishing technologies (Fig. 1). Therefore, Oliver and Pharr [1] proposed a complex phenomenological function to calculate the contact area A, denoted as A_{OP} hereafter, for a Berkovich indenter:

*Corresponding author: tel: +86 13801256332
e-mail: *gong@tsinghua.edu.cn*

$$A_{OP} = 24.5h_c^{\ 2} + C_1h_c^{\ 1} + C_2h_c^{\ 1/2} + C_3h_c^{\ 1/4} + ... + C_8h_c^{\ 1/128} \quad (4)$$

where C_1 through C_8 are constants. For the sake of convenience, we call Eq. 4 the OP area function.

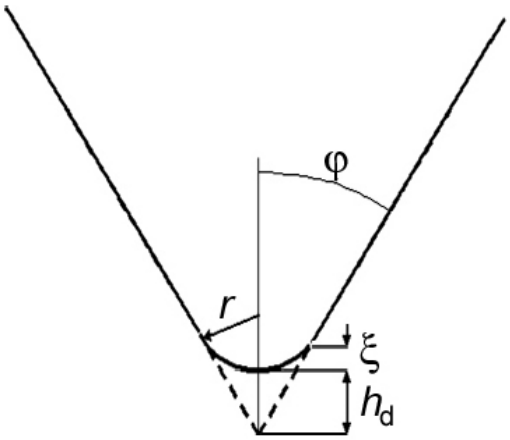

Figure 1. Schematic diagram showing the geometry of a round indenter tip

In general, the OP area function should be calibrated prior to practical tests by analysing the dependence of the contact stiffness on the contact depth based on Eq. 1 using the experimental data measured on an isotropic reference material of well-known Young's modulus, e.g. fused silica. Although the analysis technique developed by Oliver and Pharr [1] for the pre-calibration of Eq. 4 is very precise and refined, it should be pointed out that some limitations exist for the use of Eq. 4. From the viewpoint of mathematics, fitting the experimental data according to the complex form of Eq. 4 is troublesome and, in most cases, uncertainties in the fitting results would exist. For example, Sawa and Tanaka [3] found that the determination of the coefficients included in Eq. 4 is liable to the initial guess for the iteration and, as a result, it is difficult to obtain a unique area function for the same experimental data. On the other hand, the fitting results of the OP area function also depend on the depth range over which the experimental data are measured. As pointed out by Oliver and Pharr themselves [2], the pre-calibrated OP area function may be highly inaccurate outside the depth range used to construct it. Thus it is necessary to exercise caution when using the OP area function pre-calibrated within a certain depth range to analyse the experimental data measured within different depth ranges. Furthermore, several studies [3–6] have shown that the area function varies with materials even if the same indenter was used, implying that some uncertainties, although maybe very small, would exist when using the OP area function pre-calibrated with a reference material to predict the contact area for other materials. Considering all the limitations mentioned above, it seems to be convenient, and also reliable if the contact area can be determined simultaneously during, rather than prior to, a practical test.

The aim of the present study is thus to establish a new method for calculating the contact area directly from the *P-h* curve measured on the test material. The present study was based on another empirical area function [3,7,8]:

$$A_{NM} = C\left(h_c + h_d\right)^2 \quad (5)$$

where h_d is constant used to consider the fact that a real indenter is never perfect due to some tip rounding. The parameter h_d is sometimes called the truncation length of the indenter tip and its physical meaning is illustrated in Fig. 1. Note that, for the sake of convenience, we will use a subscript "NM" hereafter to represent the parameter calculated with the new method proposed in the present study.

As shown in Fig. 1, the rounded indenter tip is modelled by a rigid cone of half-included angle φ and a spherical extremity of radius r and height ξ. This model was justified by Shin *et al.* [9] who showed that experimental results can be well fitted with the analytical equations representing the cross-sectional area of a triangular-based pyramid indenter truncated by a spherical cap of various radii. Furthermore, Thurn and Cook [10] derived a two-parameter area function, similar in form to Eq. 5, based on this model for the characterisation of the depth-dependent contact area applied for a Berkovich indenter. These works theoretically confirmed the validity of Eq. 5.

Equation 5 was also employed by several authors [3,11,12] to perform the pre-calibrations of area function and frame compliance of the test machine. The procedures of pre-calibration in these works were similar to that proposed by Oliver and Pharr [1] and, therefore, many *P-h* curves measured at different peak load levels should be analysed in order to obtain a data table of (A, h_c) for extracting h_d by fitting.

Compared with the procedure proposed by Oliver and Pharr [1], Eq. 5 seems to have few special advantages except for the simplicity. Noting that Eq. 5 was employed by Malzbender *et al.* [13] to derive an analytical expression for the loading segment of nanoindentation *P-h* curve:

$$P = k^2\left(h + h_d\right)^2 \quad (6)$$

where P is the indentation load, h is the indenter displacement and the constant k is a function of the reduced modulus E_r and the hardness H:

$$k^2 = E_r\left(\frac{1}{\sqrt{C}}\sqrt{\frac{E_r}{H}} + \varepsilon\sqrt{\frac{\pi}{4}}\sqrt{\frac{H}{E_r}}\right)^{-2} \quad (7)$$

where ε is an indenter geometrical constant which takes a value of 0.75 for a Berkovich indenter [1] and C is a constant dependent only on the indenter geometry (C = 24.5 for a Berkovich indenter).

By transforming Eq. 6 in the following form:

$$P^{1/2} = k\left(h + h_d\right) \tag{8}$$

we can obtain Eq. 8 which predicts that a linear relationship exists between $P^{1/2}$ and h and, thus, h_d can be obtained from the intercept of the best-fit line.

Clearly, Eq. 8 provides a fresh and direct way to obtain the parameter h_d by analysing the loading segments of the same *P-h* curve used to extract h_c and the contact stiffness *S*. If Eq. 8 works well, the contact area would be determined directly without the need of the pre-calibration of area function. Therefore, in the present study, the efficiency of Eq. 8 in the mechanical property determination was critically examined by analysing a total of 497 *P-h* curves measured on a commercial silica glass. It will be shown that, although the resultant h_d values exhibit a significant scatter, comparable and reliable results may be obtained when using the contact area calculated based on Eqs. 5 and 8 to determine the Young's modulus and hardness.

II. Experimental

A commercial silica glass slide was selected for the present study.

A well-calibrated nanoindentation instrument (Nano Indenter G200, Agilent, Santa Clara, CA) equipped with a Berkovich indenter was used for performing the nanoindentation tests. The nanoindentation tests were performed in a force-controlled single cycle mode: the indenter was loaded gradually to the prescribed peak load, P_{max}, at a constant loading rate defined by P_{max}/t_L (where t_L is the prescribed loading time), held at peak load for a prescribed time, t_H, and then unloaded gradually at a constant unloading rate defined by P_{max}/t_L. By varying the values of P_{max} (10 ~ 400 mN), t_L (10 ~ 600 s) and t_H (10 ~ 150 s), a total of 497 tests were conducted.

Before the nanoindentation tests, the OP area function of the indenter was calibrated carefully according to the International Standard ISO 14577-2 [14] by using standard fused silica block as the reference material. The resultant area function was:

$$A_{OP} = 24.8h_c^{\,2} + 191h_c \tag{9}$$

III. Results

The loading portions of all the *P-h* curves measured in the present study were fitted according to Eq. 8. Noting that Eq. 8 holds only for $h > \xi$ [13], only the experimental data measured for $P > 0.4P_{max}$ were used for fitting. The best-fit analysis returns a correlation coefficient, *R*, larger than 0.9999 for each of the 497 measured curves, indicating that Eq. 8 is sufficiently suitable for the representation of the loading data for the nanoindentation tests.

As shown in Eq. 6, one can see that *k* is a constant dependent on the Young's modulus and hardness for a given material. Figure 2a shows the cumulative distribution function of the best-fit values of the parameter *k* included in Eq. 8. For all the 497 tests, *k* varies from 0.0085 to 0.0108 $mN^{0.5}$/nm and has an average value of 0.0102±0.0002 $mN^{0.5}$/nm (coefficient of variation is 0.015). These results indicate that, for a given material, the best-fit value of *k* can be considered to be a constant, being in agreement with the theoretical consideration. The slight variation in the best-fit *k* values may be attributed to the fact that the test material used in the present study is only a commercially available silica glass slide, rather than a well-prepared reference fused silica.

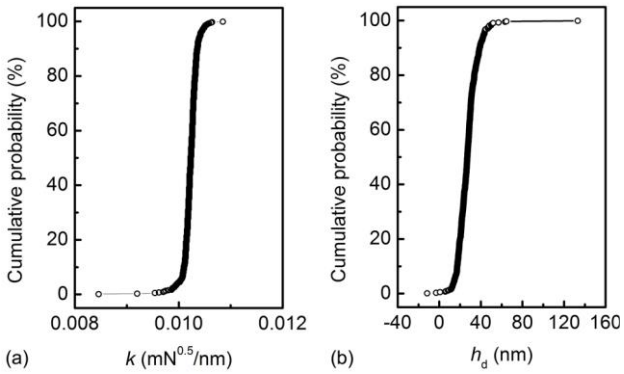

Figure 2. Cumulative distribution functions of the best-fit values of: a) *k* and b) h_d for the examined material

The cumulative distribution function (CDF) of the best-fit values of the parameter h_d is shown in Fig. 2b. Unexpectedly, larger scatter was observed in the measured h_d range (varying from –11.66 to 133.16 nm and having an average value of 27.53±10.09 nm), making it unreasonable to treat h_d as a constant. A brief discussion on such a scatter in the measured h_d will be conducted in the next section. Now it was necessary to examine the efficiency of the best-fit results given in Fig. 2b in the mechanical property determination.

The unloading portion of each considered *P-h* curve was analysed with the conventional OP method [1] to extract the contact depth h_c and the contact stiffness *S*. This was done by fitting the unloading data in the range of $0.4P_{max}$ ~ $0.95P_{max}$ according to a power law:

$$P = \alpha\left(h - h_f\right)^m \tag{10}$$

Once the fitting parameters α, m and h_f included in Eq. 10 were obtained, the contact stiffness *S* can be calculated by following equation:

$$S = \left(\frac{dP}{dh}\right)_{h=h_{max}} = \alpha m\left(h - h_f\right)^{m-1} \tag{11}$$

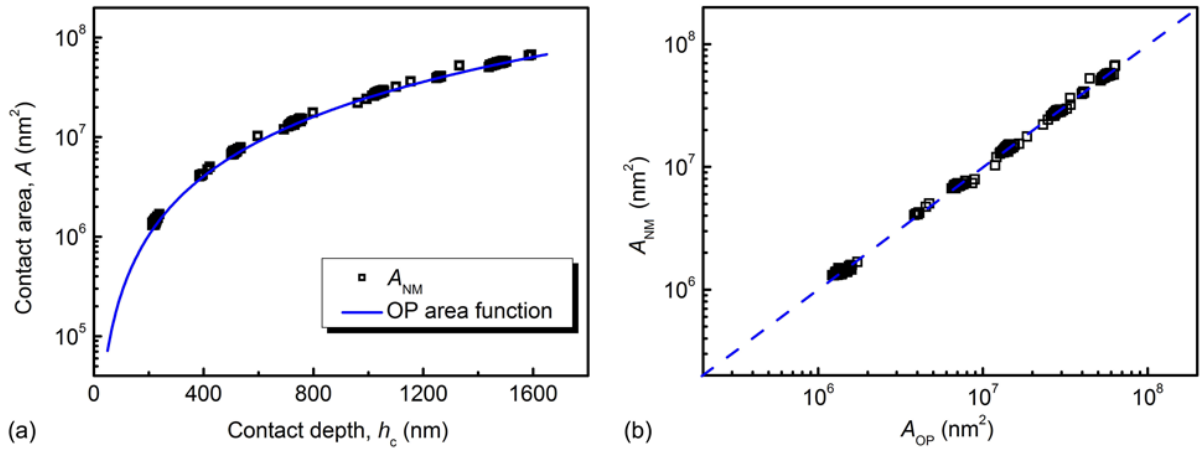

Figure 3. Comparisons between the contact areas determined with Eq. 5 and those with the pre-calibrated OP area function

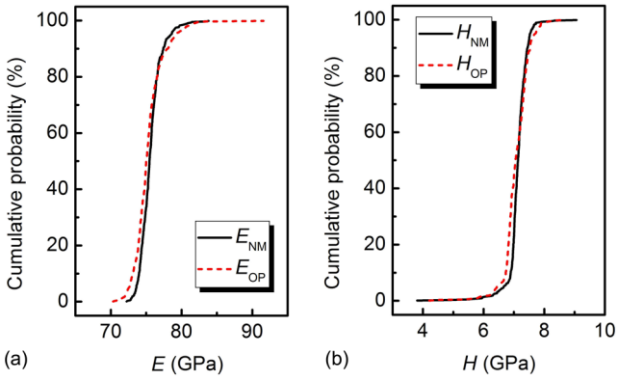

Figure 4. Cumulative distribution functions of: a) E_{NM} and E_{OP} and b) H_{NM} and H_{OP} for the examined material

$$h_c = h_{\max} - \varepsilon \frac{P_{\max}}{S} \tag{12}$$

According to International Standard ISO 14577-1 [15], the parameters $h_{\max}$ and $P_{\max}$ included in Eq. 12 are the displacement and the load, respectively, at the point at which the unloading starts, because the pre-calibration of contact area was performed using the unloading data. In the present study, however, we used the displacement and the load at the point at which the holding starts as $h_{\max}$ and $P_{\max}$ to calculate the contact area A_{NM} with Eq. 5 because the parameter h_d was determined from the loading segment, rather than unloading segment of the measured *P-h* curve.

The calculated A_{NM} is plotted as a function of h_c in Fig. 3a. The solid line predicted with the pre-calibrated OP area function is also shown in Fig. 3a. As it can be seen, all the data points fall along the solid line, implying that, within the examined range of contact depth, the resultant A_{NM}-h_c relation may also be described satisfactorily with the OP area function.

For each test, the contact area was also calculated with the pre-calibrated OP area function using h_c values determined with Eq. 12 by using the maximum displacement of the unloading segment as $h_{\max}$. The calculated A_{OP} is compared with A_{NM} in Fig. 3b. As it can be seen, there seems to be no significant difference between these two sets of data.

Using the contact area, A_{NM}, and the contact stiffness, *S*, determined respectively from the analyses of the loading and unloading segments of the same *P-h* curve, the Young's modulus E_{NM} can be calculated directly with Eqs. 1 and 2. The hardness H_{NM} can be calculated by following equation:

$$H_{NM} = \frac{P_{\max}}{A_{NM}} \tag{13}$$

The calculated results are summarised in Fig. 4. For comparison, the Young's modulus E_{OP} and hardness H_{OP} determined with the conventional OP method were also shown in Fig. 4. As it can be seen, there is only a very small statistical difference between E_{NM} and E_{OP} or between H_{NM} and H_{OP}. The average value of each parameter shown in Fig. 4 is calculated to be E_{NM} = 75.63±1.51 GPa, E_{OP} = 75.33±2.09 GPa, H_{NM} = 7.13±0.4 GPa and H_{OP} = 7.08±0.41 GPa, respectively. These experimental results clearly indicate that, from the viewpoint of statistics, the Young's modulus and the hardness determined based on A_{NM} are nearly identical to those determined with the conventional OP method.

Although good statistical agreements are observed between the results extracted with the new method proposed in the present study and those with the conventional OP method, it should be pointed out that, when examining with each test, significant differences between the two methods still exist. This can be seen in Fig. 5a, where $\Delta E/E_{NM} = (E_{OP}-E_{NM})/E_{NM}$ and $\Delta H/H_{NM} = (H_{OP}-H_{NM})/H_{NM}$ are plotted as functions of the test number. The test number used for constructing Fig. 5 is prescribed by ranking the 497 tests in the order of increasing $\Delta E/E_{NM}$.

Figure 5a indicates that, in most cases, the new method proposed in the present study would yield an *E* or *H* value different from that obtained by the conventional OP method. From the view point of

practical applications in which only a limited number of tests are performed, it is necessary to judge which value is more reliable and acceptable. Here we proposed a criterion for such a judgement based on Eq. 6. Note that the parameter k included in Eq. 6 is a function of E_r and H. By fitting the loading data according to Eq. 8, we have obtained an experimental k value for each test, see Fig. 2a. On the other hand, a "theoretical" k value, denoted as k_c, can be calculated with Eq. 7 using the determined E_r and H. In continuation of this consideration, the k_c value was calculated using the E_r and H determined with the new method and the OP method, respectively, for each test and the results are summarised in Fig. 5b. As can be seen, a larger scatter exists in $\Delta k_c^2/k^2 = (k_c^2–k^2)/k^2$ calculated with E_{OP} and H_{OP}, while the new method yields a nearly constant $\Delta k_c^2/k^2$ value for all the 497 tests, implying that, compared with the conventional OP method, the new method proposed in the present study may give more reliable and acceptable or at least self-consistent, results.

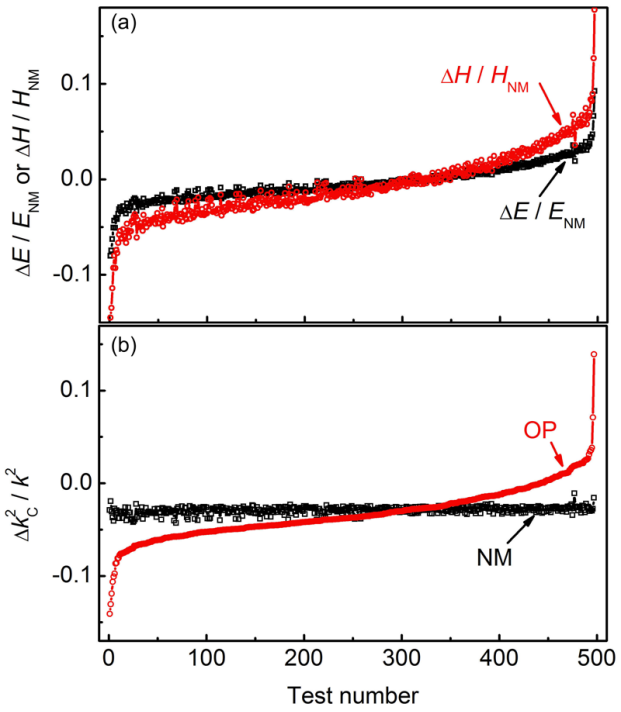

Figure 5. $\Delta E/E_{NM}$, $\Delta H/H_{NM}$, $(\Delta k_c^2/k^2)_{NM}$ and $(\Delta k_c^2/k^2)_{OP}$ measured for each test

Also, it should be noted that, as shown in Fig. 5b, the $\Delta k_c^2/k^2$-values calculated with E_{NM} and H_{NM}, $(\Delta k_c^2/k^2)_{NM}$, also exhibit a slight variation. This phenomenon may be attributed to the fact that the experimentally determined value of the exponent m included in Eq. 10 varies from test to test, resulting in a slight change in ε-value [1,2]. In addition, the average value of $(\Delta k_c^2/k^2)_{NM}$ is determined to be –0.029±0.004, i.e. the calculated $(k_c)_{NM}$ is somewhat smaller than the experimentally determined k. This may be, at least partially, attributed to the choice of β value for calculating E_r with Eq. 1 [2]. A detailed analysis of the effect of ε and β on the calculation of k_c is beyond the scope of the present study and will be conducted in the near future.

IV. Discussion

The above analyses show that the mechanical properties determined with the new method are more reliable and acceptable than those determined with the conventional OP method. The only difference between these two methods lies in the choice of the area function. In the OP method, an empirical area function is pre-calibrated prior to the practical tests using the nanoindentation data measured on a reference material, while the area function used in the new method is calibrated synchronously with the same P-h curve for mechanical property determination. This is one of main advantages of the proposed new method.

The area function, Eq. 5, selected for the new method is based on the consideration of the round indenter tip correction. Theoretically, the parameter h_d included in this area function is the truncation length of the round indenter tip (Fig. 1) and should be a constant dependent only on the indenter used. However, as shown in Fig. 2b, the experimentally determined h_d value exhibits large scatter and cannot be reasonably considered to be a constant. This experimental phenomenon warrants a further discussion.

In fact, the large scatter shown in experimentally determined h_d values was generally observed in the previous studies which used Eq. 5 to analyse the unloading segment of the measured nanoindentation P-h curves. For example, Sawa and Tanaka [3] used Eq. 5 as area function to perform the pre-calibration of frame compliance of the test machines and found that the experimentally determined h_d for a given indenter varies significantly from material to material. Similar phenomena were also reported by Gong *et al.* [16] and Troyon and Huang [11] when using Eq. 5 as area function to extract the mechanical properties of the test materials. Recently, a qualitative analysis on the variation in h_d values determined by analysing the unloading segment of the measured nanoindentation P-h curves according to Eq. 5 was conducted by Gong *et al.* [17]. By noting that previous studies have confirmed that there are many other factors (such as friction between indenter and the sample [18,19], unreliable calibration for thermal drift [20,21], loading rate [22,23], holding time [24,25], the surface roughness [26,27] of the test sample and small uncertainties in zero point calibration [28,29]), even the cleanliness of the indenter [30], pile-up [31,32] and/or sink-in behaviour during indentation, etc., may affect the measured load-displacement curve. Gong *et*

al. [17] concluded that it seems to be more reasonable to consider ($h+h_d$) included in Eq. 5 as the "true" displacement, i.e. simply considering h_d as a correction factor for the measured displacement, an integrated or statistical measure of different factors, certainly also including the effect of a round indenter tip, which may have influence on the measured displacement. This conclusion is undoubtedly suitable for the present study. In addition, it should be emphasised that, for the new method proposed in the present study, a nearly constant k was obtained (Fig. 2a), and very close to its "theoretical" value (Fig. 5b). This experimental finding provides an indirect support for the conclusion obtained by Gong *et al.* [17].

Here we provide some examples to support the above discussion by analysing the experimental data.

Figure 6a shows some typical P-h curves measured at P_{max} = 100 mN. The enlargements of these P-h curves within the displacement range of 0 ~ 300 nm are shown in Fig. 6b. As it can be seen, the P-h curves were separated from each other at the initial stage of loading. As an example, the $P^{0.5}$-h line fitted according to Eq. 8 within the range of $0.4P_{max}$ ~ $1.0P_{max}$ of the loading segment for test C is given in Fig. 6c together with the experimentally measured unloading data. Deviation of the experimental data from the prediction of Eq. 8 in the low load region is evident. Undoubtedly, such a deviation would affect the best-fit value of h_d. At least, the best-fitted $P^{0.5}$-h line will shift towards the larger h direction as the displacement occurring during the initial loading stage (say $P < 0.4P_{max}$) increases (Fig. 6d), thereby resulting in an increasing tendency in the best-fit value of h_d.

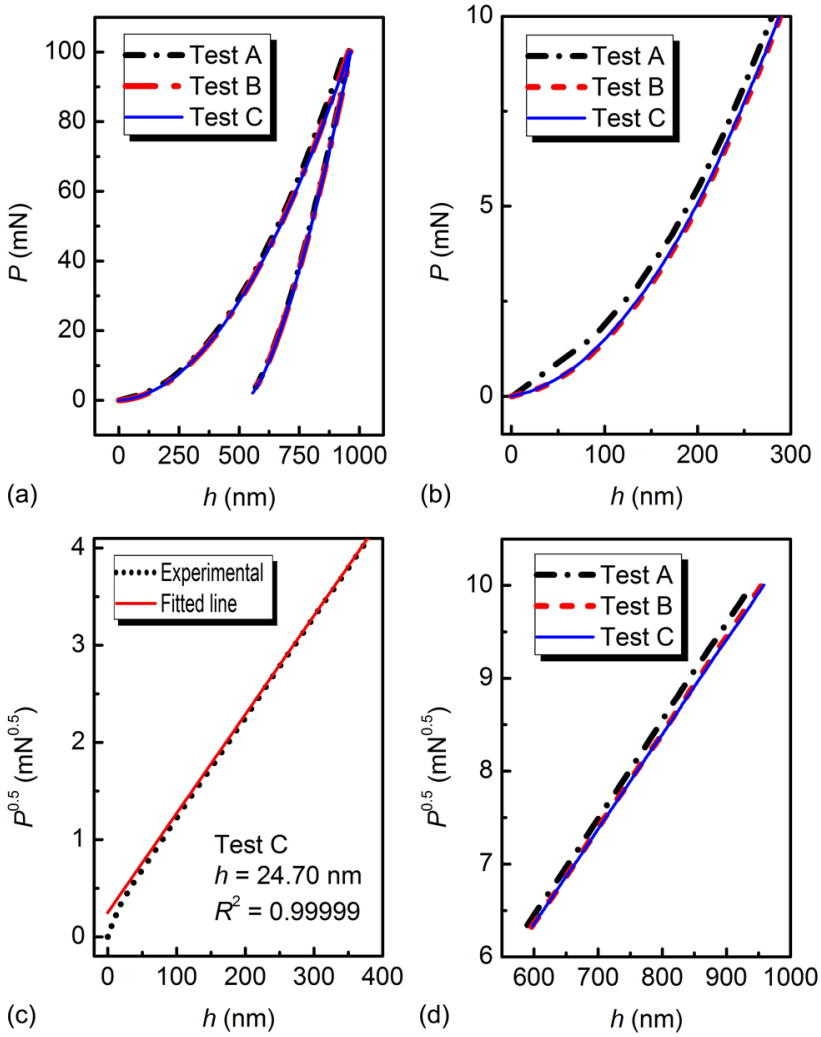

Figure 6. Some typical P-h curves measured at P_{max} = 100 mN (a); enlargements of the curves shown in (a) within the displacement range of 0 ~ 300 nm (b); comparison of the experimental loading data and fitted $P^{0.5}$-h line for test C - note that only the data in the displacement range of 0–400 nm are shown (c) and corresponding $P^{0.5}$-h relation within the range of $0.4P_{max}$ ~ $1.0P_{max}$ of the loading segment for each test (d)

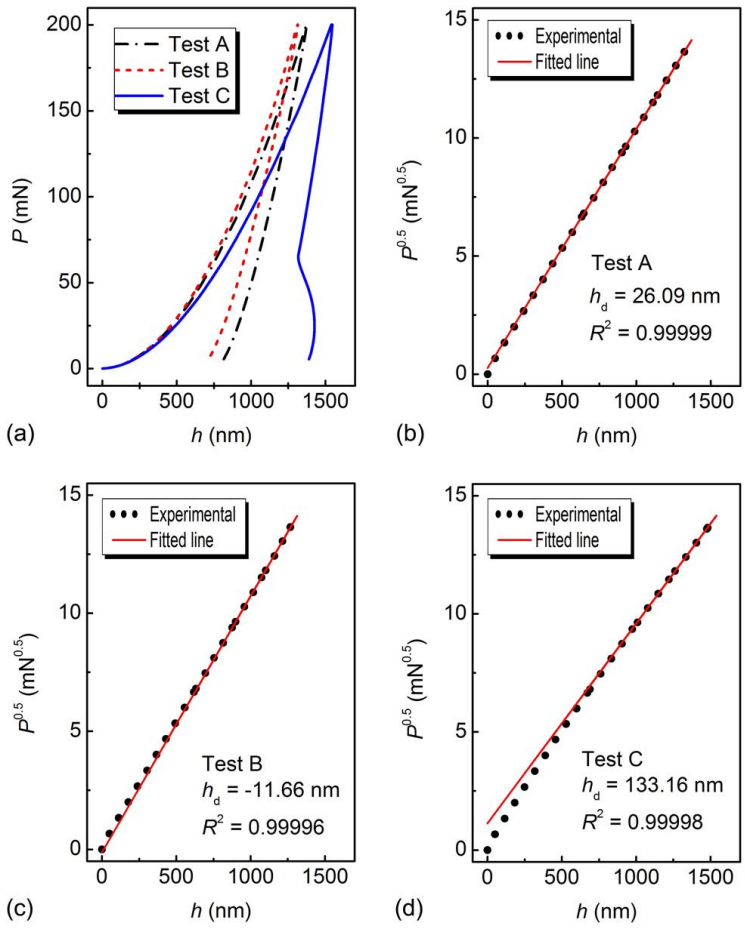

Figure 7. Some typical *P-h* curves measured at P_{max} = 200 mN and t_L = 600 s (a) and comparison of the experimental loading data and fitted $P^{0.5}$-*h* line for each test (b-d)

It should be noted that a few negative h_d values (2 of 497 tests) and extremely large (> 50 nm) h_d values (7 of 497 tests) were observed in the present study. An extreme example is given in Fig. 7. Figure 7a shows three *P-h* curves measured at P_{max} = 200 mN and t_L = 600 s. The differences between displacements at the peak load for the three tests are evident. Although excellent linear relationship between $P^{0.5}$ and *h* is observed in each case within the load range of $0.4P_{max}$ ~$1.0P_{max}$ (Figs. 7b-d), the corresponding h_d-value varies significantly: 26.09 nm for the test A, –11.66 nm for the test B and 133.16 nm for the test C, respectively. In fact, 133.16 and –11.66 nm are the maximum and minimum h_d values obtained in the present study.

It can be found by comparing Figs. 7b-d, and all the results obtained in the present study, that negative h_d values are always associated with larger displacements at the initial loading stage compared to those predicted by extrapolating the best-fitted $P^{0.5}$-*h* line. Such larger displacements during the initial loading stage may be associated with the facts that the contact site is just at or very near to a roughness peak [26,27] or a local surface tensile stress exists at the contact site [33,34]. The effect of surface roughness or the surface stress will become negligible as the displacement increases. Thus, the $P^{0.5}$-*h* relation within higher load range can be described well with Eq. 8 but the resultant h_d value may be negative.

It is of interest to note from test C that, during unloading, an abrupt increase in displacement occurs when the load decreases below about 60 mN ($0.3P_{max}$), implying that the local microstructure of the contact site of test C may be rather different from those of the tests A and B. An indirect support for this inference is the fact that, in the present study, it is the test C that yields the maximum Young's modulus, E_{NM} = 83.83 GPa and E_{OP} = 91.58 GPa and the minimum hardness, H_{NM} = 3.81 GPa (H_{OP} = 4.49 GPa is the second lowest among all the 497 H_{OP} values). As it can be seen in Fig. 7a, the local microstructural inhomogeneity around the contact site of the test C makes the displacement to increase much faster than those in the tests A and B during loading when *h* > 500 nm. It is the rapid increase in displacement that results in an extremely large h_d, 133.16 nm, for the test C.

Deviations of the experimental data from the prediction of Eq. 8 in the low load region, shown in Figs. 6c,7c,7d, were observed in most of the $P^{0.5}$-*h* lines obtained in the present study and such a deviation may be attributed to many factors including but not limited to surface roughness of the test sample,

uncertainty in zero-point calibration, etc. Due to the existence of such deviations, only the experimental data measured at $P > 0.4P_{max}$ were used for linear regression to yield k and h_d in the present study. The reason why selecting $0.4P_{max}$ as the lower bound is just that, as mentioned in Section III, the best-fit analysis according to Eq. 8 returns a correlation coefficient, R, larger than 0.9999 for each of the 497 measured curves. A further critical examination should be performed on many materials in near future to determine a reliable lower bound for linear regression.

V. Conclusions

In this paper, we proposed a new analytical method for mechanical property determination with nanoindentation tests based on the empirical area function, Eq. 5, which was established based on the consideration of the round indenter tip correction. In this method, the correction factor h_d included in Eq. 5 was determined directly by analysing the loading segment of the measured *P-h* curve and another parameter, h_c, was determined by analysing the unloading segment of the same curve. Therefore, the main advantage of this new method is that Young's modulus and hardness can be obtained directly and easily by analysing the measured *P-h* curve without the need of pre-calibration of area function.

The applicability and the reliability of the proposed new method were verified by analysing a total of 497 nanoindentation *P-h* curves measured on commercial silica glass. It was shown that, from the viewpoint of statistics, the Young's modulus and hardness extracted with the proposed method are nearly identical with those determined with the conventional OP method. It should be realised that different materials would exhibit different responses to nanoindentation. Therefore, the universality of this new method needs to be examined further by analysing the experimental data measured with different materials.

Acknowledgement: The author would like to express thanks to Ms. Lei Li of Shanghai Institute of Ceramics, CAS, China, for conducting the nanoindentation tests.

References

1. W.C. Oliver, G.M. Pharr, “An improved technique for determining hardness and elastic modulus using load and displacement sensing indentation experiments”, *J. Mater. Res*., **9** (1992) 1564–1583.
2. W.C. Oliver, G.M. Pharr, “Measurement of hardness and elastic modulus by instrumented indentation: advanced in understanding and refinements to methodology”, *J. Mater. Res*., **19** (2004) 3–20.
3. T. Sawa, K. Tanaka, “Simplified method for analyzing nanoindentation data and evaluating performance of nanoindentation instruments”, *J. Mater. Res*., **16** (2001) 3084–3096.
4. K.R. Gadelrab, F.A. Bonilla, M. Chiesa, “Densification modeling of fused silica under nanoindentation”, *J. Non-Cryst. Solids*, **358** (2012) 392–398.
5. W. Hang, L. Zhou, J. Shimuzu, J. Yuan, “A robust procedure of data analysis for micro/nano indentation”, *Prec. Eng*., **37** (2013) 408–414.
6. J. Cech, P. Hausild, O. Kovarik, A. Materna, “Examination of Berkovich indenter tip bluntness”, *Mater. Des*., **109** (2016) 347–353.
7. K. Herrmann, N.M. Jennett, W. Wegener, J. Meneve, K. Hasche, R. Seemann, “Progress in determination of the area function of indenters used for nanoindentation”, *Thin Solid Films*, **377-378** (2000) 394–400.
8. K. Herrmann, K. Hasche, F. Pohlenz, R. Seemann, “Characterisation of the geometry of indenters used for the micro- and nanoindentation method”, *Measurement*, **29** (2001) 201–207.
9. C.W. Shin, M. Yang, J.C.M. Li, “Effect of tip radius on nanoindentation”, *J. Mater. Res*., **6** (1991) 2623–2628.
10. J. Thurn, R.F. Cook, “Simplified area function for sharp indenter tips in depth-sensing indentation”, *J. Mater. Res*., **17** (2002) 1143–1146.
11. M. Troyon, L. Huang, “Correction factor for contact area in nanoindentation measurements”, *J. Mater. Res*., **20** (2005) 610–617.
12. M. Troyon, L. Huang, “Comparison of different analysis methods in nanoindentation and influence on the correction factor for contact area”, *Surf. Coat. Technol*., **201** (2006) 1613–1619.
13. J. Malzbender, G.D. With, J.D. Toonder, “The $P\text{-}h^2$ relationship in indentation”, *J. Mater. Res*., **15** (2000) 1209-1212.
14. ISO 14577-2 Standard, “Metallic materials - Instrumented indentation test for hardness and materials parameters - Part 2: Verification and calibration of test machines”, 2015.
15. ISO 14577-1 Standard, “Metallic materials - Instrumented indentation test for hardness and materials parameters - Part 1: Test method”, 2015.
16. J.H. Gong, H.Z. Miao, Z.J. Peng, “Analysis of the nanoindentation data measured with a Berkovich indenter for brittle materials: effect of the residual contact stress”, *Acta Mater*., **52** (2004) 785–793.
17. J.H. Gong, B. Deng, D.Y. Jiang, “On the efficiency of the "effective truncation length" of indenter tip in mechanical property determination with nanoindentation tests”, *Mater. Today Comm*., **25** (2020) 101412.
18. M. Mata, J. Alcala, “The role of friction on sharp indentation”, *J. Mech. Phys. Solids*, **52** (2004) 145–165.
19. S.C. Bellemare, M. Dao, S. Suresh, “Effects of mechanical properties and surface friction on elasto-plastic sliding contact”, *Mech. Mater*., **40** (2008) 206–219.
20. A.L. Romasco, L.H. Friedman, L. Fang, R.A. Meirom, T.C. Clark, R. Polcawich, J. Pulskamp, M. Dubey, C.L. Muhlstein, “Practical implications of instrument displacement drift during force-controlled nanoindentation”, *J. Test. Eval*., **38** (2010) 203–210.
21. S. Verma, P. Sarkar, P. Pant, “Thermal drift in room temperature nanoindentation experiments: measurement and correction”, *J. Mater. Res*., **36** (2021) 3436–3444.

22. R. Limbach, B.P. Rodrigues, L. Wondraczek, “Strain-rate sensitivity of glasses”, *J. Non-Cryst. Solids*, **404** (2015) 124–134.
23. V. Maier-Kiener, K. Durst, “Advanced nanoindentation testing for studying strain-rate sensitivity and activation volume”, *J. Optoelect. Mater.*, **69** (2015) 2246–2255.
24. T. Chudoba, F. Richter, “Investigation of creep behavior under load during indentation experiments and it influence on hardness and modulus results”, *Surf. Coat. Technol*., **148** (2001) 191–198.
25. M.I. Simoes, J.V. Fernandes, A. Cavaleiro, “The influence of experimental parameters on hardness and Young's modulus determination using depth-sensing testing”, *Phil. Mag. A*, **82** (2002) 1911–1919.
26. K.D. Bouzakis, N. Michailidis, S. Hadjiyiannis, G. Skordaris, G. Erkens, “The effect of specimen roughness and indenter tip geometry on the determination accuracy of thin hard coatings stress-strain laws by nanoindentation”, *Mater. Charact*., **49** (2003) 149–156.
27. J.Y. Kim, S.K. Kang, J.J. Lee, J.I. Jang, Y.H. Lee, D. Kwon, “Influence of surface-roughness on indentation size effect”, *Acta Mater*., **55** (2007) 3555–3562.
28. Y.F. Cao, D.H. Yang, W. Soboyejoy, “Nanoindentation method for determining the initial contact and adhesion characteristics of soft polydimethylsiloxane”, *J. Mater. Res*., **20** (2005) 2004–2011.
29. S.R. Kalidindi, S. Pathak, “Determination of the effective zero-point and the extraction of spherical nanoindentation stress-strain curves”, *Acta Mater*., **14** (2008) 3523–3532.
30. J.E. Jakes, “Improved methods for nanoindentation Berkovich probe calibrations using fused silica”, *J. Mater. Sci*., **53** (2018) 4814–4827.
31. A. Bolshakov, G.M. Pharr, “Influences of pileup on the measurement of mechanical properties by load and depth sensing indentation techniques”, *J. Mater. Res.*, **14** (1999) 1049–1058.
32. K.O. Kese, Z.C. Li, B. Bergman, “Method to account for true contact area in soda-lime glass during nanoindentation with the Berkovich tip”, *Mater. Sci. Eng. A*, **404** (2005) 1–8.
33. T.Y. Tsui, W.C. Oliver, G.M. Pharr, “Influences of stress on the measurement of mechanical properties using nanoindentation: I, experimental studies in an aluminum alloys”, *J. Mater. Res*., **11** (1996) 752–759.
34. Z.H. Xu, X.D. Li, “Influence of equi-biaxial residual stress on unloading behavior of nanoindentation”, *Acta Mater*., **53** (2005) 1913–1919.